

Linearized reflection coefficient and reflectivity modeling in fractured and attenuative reservoirs

Huaizhen Chen, Kristopher Innanen

ABSTRACT

Based on the complex linear slip theory, we derive complex stiffness parameters in terms of fracture weaknesses and induced attenuation factor under the assumption of the host rock being elastic and isotropic. Incorporating with the attenuative crack model, we relate the induced attenuation factor to fracture properties (fracture density and aspect ratio) and fluid parameters (fluid bulk modulus and viscosity), and study how fracture density and water saturation affect the variation of the induced factor in seismic frequency range (1-100 Hz). Using perturbations in the complex stiffness parameters, we derive a complex linearized reflection coefficient involving the induced attenuation factor and fracture weaknesses. The accuracy of the derived reflection coefficient is confirmed by comparing the result calculated using the extended reflectivity method and that computed using the derived equation. We finally use the derived linearized reflection coefficient to obtain the seismic reflection response for the case of fractured reservoirs with different values of fracture density and water saturation. We conclude that the attenuation factor is applicable to distinguishing between oil-bearing and water-bearing reservoirs, and seismic response difference induced by fracture density and water saturation increases with the incidence angle.

INTRODUCTION

Seismic wave propagating through a rock with a set of parallel vertical fractures exhibits the horizontal transverse isotropy (HTI). The linear-slip model (Schoenberg and Douma, 1988; Schoenberg and Sayers, 1995) and the penny-shaped crack model (Hudson, 1980) are combined to relate stiffness parameters of the fractured rock to fracture properties (fracture density, aspect ratio and filling moduli). In the linear-slip model, the normal and tangential fracture weaknesses are defined to measure the influence of fracture properties on the stiffness parameters. Much work has been done to demonstrate that fluid viscosity and the movement of fluid between the connected pores via the fractures can generate energy losses when seismic wave propagates in fractured rocks. Chapman (2003) proposed a fractured rock model under the assumption of perfect fluid pressure equalization between the fractures and equant porosity, and studied frequency-dependent anisotropy due to meso-scale fractures. Gurevich (2003) derived a set of equations to analyze elastic properties of saturated porous rocks with aligned fractures. Brajanovski et al. (2006) studied seismic attenuation due to wave-induced fluid flow in fractured porous media. Galvin and Gurevich (2009) considered fractures to be thin circular cracks to simulate how fractures affect the elastic properties, and estimated the attenuation and dispersion of elastic waves propagating in fractured rocks. Tang et al. (2012) proposed a cracked porous medium elastic wave theory, which can be applied to identify hydrocarbons from the acoustic measurement data. Kong et al. (2013) studied effect of fracture fill on seismic attenuation and dispersion in fractured porous rocks.

In addition to seismic wave anisotropy and attenuation, Carcione (1992) demonstrated that a HTI medium exhibits quality factor (Q) anisotropy. Carcione (2000) proposed a model for source rocks, which can relate seismic anisotropy (in velocity and attenuation) to kerogen content, pore pressure, and water saturation. Chichinina et al. (2006, 2009) extended the linear-slip model to study the attenuation anisotropy in fractured media, and presented P-wave and S-wave inverse quality factors related to the normal and tangential fracture weaknesses. Carcione et al. (2012) studied fracture-induced anisotropic attenuation and derived compliance and stiffness matrices of the fractured rock in terms of the complex normal and tangential fracture compliances for the HTI and orthorhombic media. Carcione et al. (2013) proposed characteristics of angular and frequency-dependent wave velocity and attenuation in the fractured rock with a high permeability. Based on anisotropic quality factors, Zhu (2017) simulated seismic wave propagation in viscoelastic anisotropic media using frequency-independent Q wave equation.

Using the complex linear-slip model (Chichinina et al., 2006), we first propose expressions of the complex stiffness parameters in terms of fracture weaknesses and attenuation factor. Incorporating with the attenuative crack model, we relate the attenuation factor to fracture properties (fracture density and aspect ratio) and fluid parameters (fluid bulk modulus and viscosity), and we analyze how the attenuation factor is influenced by fracture density and water saturation. Using a scattering function involving slowness and polarization of PP-wave wave, we derive an linearized reflection coefficient as a function of fracture weaknesses and attenuation factor. In order to verify the accuracy of the derived reflection coefficient, we compare the result calculated using the derived reflection coefficient and that computed using the extended reflectivity modeling method. Our work ends with the modeling of reflection response for the case of fractured reservoirs with different values of fracture density and water saturation.

THEORY AND METHOD

Stiffness matrix related to induced attenuation

Based on the linear slip theory (Schoenberg and Douma, 1988; Schoenberg and Sayers, 1995), Chichinina et al. (2006) proposed a complex stiffness matrix for a homogeneous and isotropic host rock with a set of parallel fractures whose normals parallel to the x_1 -axis

$$\tilde{\mathbf{C}} = \begin{bmatrix} M(1 - \widetilde{\Delta}_N) & \lambda(1 - \widetilde{\Delta}_N) & \lambda(1 - \widetilde{\Delta}_N) & 0 & 0 & 0 \\ \lambda(1 - \widetilde{\Delta}_N) & M(1 - \chi^2 \widetilde{\Delta}_N) & \lambda(1 - \chi \widetilde{\Delta}_N) & 0 & 0 & 0 \\ \lambda(1 - \widetilde{\Delta}_N) & \lambda(1 - \chi \widetilde{\Delta}_N) & M(1 - \chi^2 \widetilde{\Delta}_N) & 0 & 0 & 0 \\ 0 & 0 & 0 & \mu & 0 & 0 \\ 0 & 0 & 0 & 0 & \mu(1 - \widetilde{\Delta}_T) & 0 \\ 0 & 0 & 0 & 0 & 0 & \mu(1 - \widetilde{\Delta}_T) \end{bmatrix}, \quad (1)$$

where $M = \lambda + 2\mu$, $\chi = \lambda/M = 1 - 2g$, $g = \mu/M$, λ and μ are Lamé constants of the homogeneous isotropic and elastic host rock, and $\widetilde{\Delta}_N$ and $\widetilde{\Delta}_T$ are the complex normal and

tangential fracture weaknesses, which are given by (Chichinina et al., 2006, 2009)

$$\begin{aligned}\widetilde{\Delta}_N &= \Delta_N - i\Delta_N^I, \\ \widetilde{\Delta}_T &= \Delta_T - i\Delta_T^I,\end{aligned}\tag{2}$$

where Δ_N and Δ_T , and Δ_N^I and Δ_T^I are the real and imaginary parts of the complex fracture weaknesses, respectively.

Carcione (2000) presented the inverse quality factor $1/Q$ for each stiffness parameter of an anisotropic and attenuative medium

$$\frac{1}{Q} = \frac{\text{Im}(\widetilde{C}_{mn})}{\text{Re}(\widetilde{C}_{mn})},\tag{3}$$

where Re and Im denote the real and imaginary parts of the stiffness parameter, and \widetilde{C}_{mn} represents the element of the complex stiffness matrix.

Combining equations 1 and 3, we present an inverse quality factor matrix for the fractured and attenuative medium

$$\frac{1}{\mathbf{Q}} = \begin{bmatrix} 1/Q_{11} & 1/Q_{12} & 1/Q_{12} & 0 & 0 & 0 \\ 1/Q_{12} & 1/Q_{33} & 1/Q_{23} & 0 & 0 & 0 \\ 1/Q_{12} & 1/Q_{23} & 1/Q_{33} & 0 & 0 & 0 \\ 0 & 0 & 0 & 1/Q_{44} & 0 & 0 \\ 0 & 0 & 0 & 0 & 1/Q_{55} & 0 \\ 0 & 0 & 0 & 0 & 0 & 1/Q_{55} \end{bmatrix},\tag{4}$$

where

$$\begin{aligned}\frac{1}{Q_{11}} &= \frac{\text{Im}[M(1 - \widetilde{\Delta}_N)]}{\text{Re}[M(1 - \widetilde{\Delta}_N)]} = \frac{\Delta_N^I}{1 - \Delta_N}, \\ \frac{1}{Q_{12}} &= \frac{1}{Q_{13}} = \frac{1}{Q_{21}} = \frac{1}{Q_{31}} = \frac{1}{Q_{11}}, \\ \frac{1}{Q_{22}} &= \frac{\text{Im}[M(1 - \chi^2 \widetilde{\Delta}_N)]}{\text{Re}[M(1 - \chi^2 \widetilde{\Delta}_N)]} = \frac{(1 - 2g)^2 \Delta_N^I}{1 - (1 - 2g)^2 \Delta_N}, \\ \frac{1}{Q_{23}} &= \frac{\text{Im}[\lambda(1 - \chi \widetilde{\Delta}_N)]}{\text{Re}[\lambda(1 - \chi \widetilde{\Delta}_N)]} = \frac{(1 - 2g) \Delta_N^I}{1 - (1 - 2g) \Delta_N}, \\ \frac{1}{Q_{33}} &= \frac{1}{Q_{22}}, \quad \frac{1}{Q_{32}} = \frac{1}{Q_{23}}, \quad \frac{1}{Q_{44}} = 0, \\ \frac{1}{Q_{55}} &= \frac{\text{Im}[\mu(1 - \widetilde{\Delta}_T)]}{\text{Re}[\mu(1 - \widetilde{\Delta}_T)]} = \frac{\Delta_T^I}{1 - \Delta_T}, \quad \frac{1}{Q_{66}} = \frac{1}{Q_{55}}.\end{aligned}\tag{5}$$

Combining equations 4 and 5, we use two inverse quality factors $1/Q_N = 1/Q_{11}$ and

$1/Q_T = 1/Q_{55}$ to rewrite the complex normal and tangential fracture weaknesses

$$\begin{aligned}\widetilde{\Delta}_N &= \Delta_N - i \frac{1}{Q_N} (1 - \Delta_N), \\ \widetilde{\Delta}_T &= \Delta_T - i \frac{1}{Q_T} (1 - \Delta_T).\end{aligned}\quad (6)$$

Substituting equation 6 into equation 1, we re-express the complex stiffness parameters

$$\begin{aligned}\widetilde{C}_{11} &= M \left[1 - \Delta_N + i \frac{1}{Q_N} (1 - \Delta_N) \right], \\ \widetilde{C}_{12} &= \lambda \left[1 - \Delta_N + i \frac{1}{Q_N} (1 - \Delta_N) \right], \\ \widetilde{C}_{23} &= \lambda \left[1 - (1 - 2g)\Delta_N + i \frac{1}{Q_N} (1 - 2g)(1 - \Delta_N) \right], \\ \widetilde{C}_{33} &= \lambda \left[1 - (1 - 2g)^2 \Delta_N + i \frac{1}{Q_N} (1 - 2g)^2 (1 - \Delta_N) \right], \\ \widetilde{C}_{44} &= \mu, \widetilde{C}_{55} = \mu \left[1 - \Delta_T + i \frac{1}{Q_T} (1 - \Delta_T) \right].\end{aligned}\quad (7)$$

Hudson et al. (1996) proposed an effective model to calculate stiffness matrix for an elastic solid with thin, penny-shaped ellipsoidal cracks

$$\widetilde{\mathbf{C}} = \begin{bmatrix} M(1 - \frac{M}{M} e \widetilde{U}_{33}) & \lambda(1 - \frac{M}{M} e \widetilde{U}_{33}) & \lambda(1 - \frac{M}{M} e \widetilde{U}_{33}) & 0 & 0 & 0 \\ \lambda(1 - \frac{\mu}{M} e \widetilde{U}_{33}) & M(1 - \frac{\mu}{\lambda \chi} e \widetilde{U}_{33}) & \lambda(1 - \frac{\mu}{\lambda} e \widetilde{U}_{33}) & 0 & 0 & 0 \\ \lambda(1 - \frac{\mu}{M} e \widetilde{U}_{33}) & \lambda(1 - \frac{\mu}{\lambda} e \widetilde{U}_{33}) & M(1 - \frac{\mu}{\lambda \chi} e \widetilde{U}_{33}) & 0 & 0 & 0 \\ 0 & 0 & 0 & \mu & 0 & 0 \\ 0 & 0 & 0 & 0 & \mu(1 - e \widetilde{U}_{11}) & 0 \\ 0 & 0 & 0 & 0 & 0 & \mu(1 - e \widetilde{U}_{11}) \end{bmatrix}, \quad (8)$$

where e is the fracture density, and in the case of an equant porosity model, U_{11} and U_{33} are given by (Pointer et al., 2000)

$$\begin{aligned}\widetilde{U}_{11} &= \frac{16}{3(3 - 2g)} \frac{1}{1 + \Psi(\omega)}, \\ \widetilde{U}_{33} &= \frac{4}{3(1 - g)} \frac{1}{1 + \Upsilon(\omega)},\end{aligned}\quad (9)$$

and in the case of fluid saturated cracks, Ψ and Υ are expressed as

$$\begin{aligned}\Psi(\omega) &= \frac{4i\omega\eta_f}{\pi \mu} \frac{1}{3 - 2g}, \\ \Upsilon(\omega) &= \frac{1}{\pi c} \frac{aK_f}{\mu} \frac{1}{1 - g} \frac{1}{1 + 3(1 - i)J/(2c)},\end{aligned}\quad (10)$$

where c/a is the fracture aspect ratio, K_f is the bulk moduli of fluid, η_f is the fluid viscosity, ω is the angular frequency, and the quantity J is related to the host rock permeability P_m , the host rock porosity ϕ_h , the fluid viscosity η_f and the bulk modulus of the fillings K_f

$$J = \sqrt{\frac{\omega \phi_h K_f P_m}{2\eta_f}}. \quad (11)$$

Pointer et al. (2000) pointed out that in the case of seismic frequency range (1-100 Hz), $\Psi(\omega) \approx 0$. Hence, \tilde{U}_{11} is real in the seismic frequency range. Combining equations 1 and 8, we re-express the complex normal and tangential fracture weaknesses in terms of \tilde{U}_{11} and \tilde{U}_{33} , which relates the inverse quality factors $1/Q_N$ and $1/Q_T$ to fracture properties and fluid parameters

$$\tilde{\Delta}_N = \frac{M}{\mu} e \tilde{U}_{33},$$

$$\tilde{\Delta}_T = \frac{16e}{3(3-2g)},$$

$$\frac{1}{Q_N(\omega)} = \frac{\text{Im} \left(\frac{M}{\mu} \tilde{U}_{33} e \right)}{1 - \text{Re} \left(\frac{M}{\mu} \tilde{U}_{33} e \right)},$$

$$\frac{1}{Q_T} = 0. \quad (12)$$

We observe that the fracture-induced attenuation factor $1/Q_N$ is frequency-dependent. Combining equations 9-12, we may analyze how fracture properties and fluid parameters affect the induced attenuation.

Linearized P-to-P reflection coefficient in fractured and attenuative media

Using the complex stiffness parameters shown in equation 7, we first express perturbations in complex stiffness parameters for the case of an interface separating an isotropic and elastic medium and a fractured and attenuative medium.

Taking \tilde{C}_{11} as an example

$$\begin{aligned} \Delta \tilde{C}_{11} &= \left(M + \frac{\Delta M}{2} \right) \left[1 - \Delta_N + i \frac{1}{Q_N} (1 - \Delta_N) \right] - \left(M - \frac{\Delta M}{2} \right) \\ &= \Delta M - \left(M + \frac{\Delta M}{2} \right) \Delta_N + i \frac{1}{Q_N} \left(M + \frac{\Delta M}{2} \right) (1 - \Delta_N), \end{aligned} \quad (13)$$

where M is the average value of P-wave modulus for the upper and lower media, and ΔM is change in P-wave modulus across the interface. The perturbations in other stiffness parameters are expressed as

$$\begin{aligned}
\Delta\tilde{C}_{12} &= \Delta\lambda - \left(\lambda + \frac{\Delta\lambda}{2}\right) \Delta_N + i\frac{1}{Q_N} \left(\lambda + \frac{\Delta\lambda}{2}\right) (1 - \Delta_N), \\
\Delta\tilde{C}_{23} &= \Delta\lambda - (1 - 2g) \left(\lambda + \frac{\Delta\lambda}{2}\right) \Delta_N \\
&\quad + i\frac{1}{Q_N} \left(\lambda + \frac{\Delta\lambda}{2}\right) (1 - 2g) (1 - \Delta_N), \\
\Delta\tilde{C}_{33} &= \Delta M - (1 - 2g)^2 \left(M + \frac{\Delta M}{2}\right) \Delta_N \\
&\quad + i\frac{1}{Q_N} \left(M + \frac{\Delta M}{2}\right) (1 - 2g)^2 (1 - \Delta_N), \\
\Delta\tilde{C}_{44} &= \Delta\mu, \Delta\tilde{C}_{55} = \Delta\mu - \left(\mu + \frac{\Delta\mu}{2}\right) \Delta_T,
\end{aligned} \tag{14}$$

where $\Delta\lambda$ and $\Delta\mu$ are changes in Lamé constants across the reflection interface, and λ and μ are the average values of Lamé constants for the upper and lower media.

The relationship between PP-wave reflection coefficient R_{PP} and the scattering function S involving the perturbation in stiffness is given by (Shaw and Sen, 2004, 2006)

$$R_{PP} = \frac{1}{4\rho \cos^2 \theta} S = \frac{1}{4\rho \cos^2 \theta} \left(\Delta\rho \cos 2\theta + \sum_{m=1, n=1}^{m=6, n=6} \Delta\tilde{C}_{mn} \xi_{mn} \right), \tag{15}$$

where ρ is the average value of density for the upper and lower media, θ is the P-wave incidence angle, and ξ_{mn} is related to slowness and polarization of the wave. Elements of ξ_{mn} used to derive the linearized reflection coefficient are given by (Shaw and Sen, 2006)

$$\begin{aligned}
\xi_{11} &= \frac{\sin^4 \theta \cos^4 \varphi}{\alpha^2}, \xi_{12} = \frac{\sin^4 \theta \sin^2 \varphi \cos^2 \varphi}{\alpha^2}, \xi_{13} = \frac{\sin^2 \theta \cos^2 \theta \cos^2 \varphi}{\alpha^2}, \\
\xi_{21} &= \xi_{12}, \xi_{22} = \frac{\sin^4 \theta \sin^4 \varphi}{\alpha^2}, \xi_{23} = \frac{\sin^2 \theta \cos^2 \theta \sin^2 \varphi}{\alpha^2}, \\
\xi_{31} &= \xi_{13}, \xi_{32} = \xi_{23}, \xi_{33} = \cos^4 \theta, \xi_{44} = \frac{-4\sin^2 \theta \cos^2 \theta \sin^2 \varphi}{\alpha^2}, \\
\xi_{55} &= \frac{-4\sin^2 \theta \cos^2 \theta \cos^2 \varphi}{\alpha^2}, \xi_{66} = \frac{4\sin^4 \theta \sin^2 \varphi \cos^2 \varphi}{\alpha^2},
\end{aligned} \tag{16}$$

where φ is the azimuthal angle of the seismic line with respect to the symmetry axis of fractures, and α is P-wave velocity of the elastic and isotropic host rock. Both the incidence and azimuthal angles are the phase angles (Chen et al., 2017a,b).

Combining equations 13-16, we derive the frequency-dependent linearized P-to-P complex reflection coefficient

$$\begin{aligned}
 R_{\text{PP}}(\theta, \varphi, \omega) = & a_M(\theta)R_M + a_\mu(\theta)R_\mu + a_\rho(\theta)R_\rho \\
 & + a_{\Delta_N}(\theta, \varphi)\Delta_N + a_{\Delta_T}(\theta, \varphi)\Delta_T \\
 & + a_{Q_N}(\theta, \varphi)\frac{i}{Q_N},
 \end{aligned} \tag{17}$$

where

$$\begin{aligned}
 a_M(\theta) &= \frac{1}{2 \cos^2 \theta}, a_\mu(\theta) = -4g \sin^2 \theta, a_\rho(\theta) = 1 - \frac{1}{2 \cos^2 \theta}, \\
 a_{\Delta_N}(\theta, \varphi) &= -\frac{1}{4 \cos^2 \theta} [1 - 2g (\sin^2 \theta \sin^2 \varphi + \cos^2 \theta)]^2, \\
 a_{\Delta_T}(\theta, \varphi) &= -g \tan^2 \theta \cos^2 \varphi (\sin^2 \theta \sin^2 \varphi - \cos^2 \theta), \\
 a_{Q_N}(\theta, \varphi) &= -a_{\Delta_N}(\theta, \varphi),
 \end{aligned} \tag{18}$$

and where $R_M = \Delta M/(2M)$ and $R_\mu = \Delta \mu/(2\mu)$ are reflectivities of P- and S-wave moduli of the elastic and isotropic host rock, and $R_\rho = \Delta \rho/(2\rho)$ is the density reflectivity. It is important to stress that under the assumptions of small relative changes in P- and S-wave moduli, weak fracture weaknesses and low attenuation factor, we neglect the term proportional to R_M/Q_N , $R_M \Delta_N$ and $R_\mu \Delta_T$ in the derivation of the linearized reflection coefficient. After the calculation of the frequency-dependent reflection coefficient, we may compute the reflection coefficient in time domain using the inverse Fourier transform.

Extended reflectivity modeling method in fractured and attenuative media

In order to testify the accuracy of the derived reflection coefficient, we compare the result calculated using equation 17 and that computed using the reflectivity modeling method extended to fractured and attenuative media. We next present the detailed process to calculate PP-wave reflection coefficient using the extended reflectivity modeling method. Figure 1 shows a three-layer model, in which the upper and lower layers are elastic and isotropic, and the middle layer is fractured and attenuative.

The displacement functions of the incidence P-wave (u_{iP}), the reflection P-wave (u_{P_2}), and the reflection S-wave (u_{S_2}) in layer 3 are given by

$$\begin{aligned}
 u_{iP} &= A_{iP} \exp [i (k_x x - \omega t)] \exp (-ik_z^{P_3} z), \\
 u_{rP_3} &= A_{rP_3} \exp [i (k_x x - \omega t)] \exp (ik_z^{P_3} z), \\
 u_{rS_3} &= B_{rS_3} \exp [i (k_x x - \omega t)] \exp (ik_z^{S_3} z),
 \end{aligned} \tag{19}$$

where A_{iP} , A_{rP_3} and B_{rS_3} are amplitudes of the incident P-wave, the reflected P-wave and the reflected S-wave, $k_x = \frac{\omega}{p}$, $p = \frac{V_{P_3}}{\sin \theta_{P_3}} = \frac{V_{S_3}}{\sin \theta_{S_3}}$, $k_z^{P_3} = \frac{k_x}{\tan \theta_{P_3}}$, $k_z^{S_3} = \frac{k_x}{\tan \theta_{S_3}}$, V_{P_3} and V_{S_3} are P- and S-wave velocities of the layer 3, θ_{P_3} and θ_{S_3} are angles of P-wave incidence and S-wave reflection, t is the time, and z is the depth.

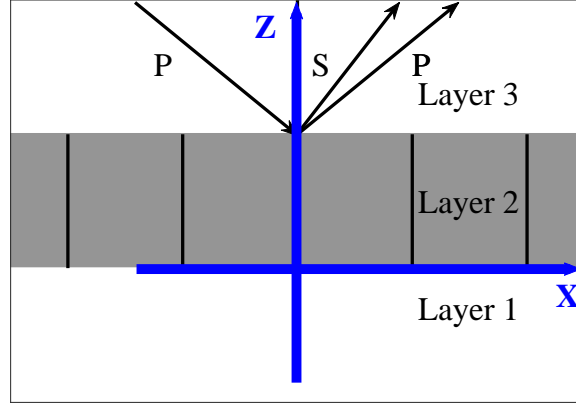


FIG. 1. An reflection interface separating an elastic and isotropic medium and a fractured and attenuative medium.

For the fractured and attenuative layer, the displacement functions of P- and S-wave (u_{P_2} and u_{S_2}) are expressed as

$$\begin{aligned} u_{P_2} &= [A_{tP_2} \exp(-ik_z^{P_2} z) + A_{rP_2} \exp(ik_z^{P_2} z)] \exp[i(k_x x - \omega t)], \\ u_{S_2} &= [B_{tS_2} \exp(-ik_z^{S_2} z) + B_{rS_2} \exp(ik_z^{S_2} z)] \exp[i(k_x x - \omega t)], \end{aligned} \quad (20)$$

where A_{tP_2} and A_{rP_2} are amplitudes of the transmitted P-wave and the reflected P-wave respectively, B_{tS_2} and B_{rS_2} are amplitudes of the transmitted S-wave and the reflected S-wave respectively, $k_z^{P_2} = \frac{k_x}{\tan\theta_{P_2}}$, $k_z^{S_2} = \frac{k_x}{\tan\theta_{S_2}}$, and θ_{P_2} and θ_{S_2} are angles of P-wave reflection and S-wave reflection.

For the lower layer, the displacement functions of P-wave (u_{P_1}) and S-wave (u_{S_1}) are given by

$$\begin{aligned} u_{P_1} &= A_{tP_1} \exp[i(k_x x - \omega t)] \exp(-ik_z^{P_1} z), \\ u_{S_1} &= B_{tS_1} \exp[i(k_x x - \omega t)] \exp(-ik_z^{S_1} z), \end{aligned} \quad (21)$$

where A_{tP_1} is the transmitted P-wave amplitude, B_{tS_1} is the transmitted S-wave amplitude, $k_z^{P_1} = \frac{k_x}{\tan\theta_{P_1}}$, $k_z^{S_1} = \frac{k_x}{\tan\theta_{S_1}}$, and θ_{P_1} and θ_{S_1} are angles of P- and S-wave transmissions in the lower layer.

We present x - and z -components of displacement (D_x and D_z) and stress (S_x and S_z)

$$\begin{aligned} D_x &= \frac{\partial u_P}{\partial x} - \frac{\partial u_S}{\partial z}, \\ D_z &= \frac{\partial u_P}{\partial z} + \frac{\partial u_S}{\partial x}, \\ S_x &= \lambda \left(\frac{\partial D_x}{\partial x} + \frac{\partial D_z}{\partial z} \right) + 2\mu \frac{\partial D_z}{\partial z}, \\ S_z &= \mu \left(\frac{\partial D_x}{\partial z} + \frac{\partial D_z}{\partial x} \right), \end{aligned} \quad (22)$$

where λ and μ are Lamé constants of the corresponding layer.

For the lower interface of the layer 3 ($u_P = u_{iP} + u_{rP3}$ and $u_S = 0$), we obtain x - and z -components of displacement (D_{x3} and D_{z3}) and stress (S_{x3} and S_{z3})

$$\begin{bmatrix} D_{x3} \\ D_{z3} \\ S_{x3} \\ S_{z3} \end{bmatrix} = G_3^{z=h} \begin{bmatrix} A_{rP3} + A_{iP} \\ A_{rP3} - A_{iP} \\ B_{rS3} \\ B_{rS3} \end{bmatrix} \exp [i (k_x x - \omega t)], \quad (23)$$

where

$$G_3^{z=h} = \begin{bmatrix} ik_x \cos(k_z^{P3} h) & -k_x \sin(k_z^{P3} h) & -ik_z^{S3} \cos(k_z^{S3} h) & k_z^{S3} \sin(k_z^{S3} h) \\ -k_z^{P3} \sin(k_z^{P3} h) & ik_z^{P3} \cos(k_z^{P3} h) & -k_x \sin(k_z^{S3} h) & ik_x \cos(k_z^{S3} h) \\ -\Omega_3 \cos(k_z^{P3} h) & -i\Omega_3 \sin(k_z^{P3} h) & -2\mu_3 k_x k_z^{S3} \cos(k_z^{S3} h) & -2i\mu_3 k_x k_z^{S3} \sin(k_z^{S3} h) \\ -2i\mu_3 k_x k_z^{P3} \sin(k_z^{P3} h) & -2\mu_3 k_x k_z^{P3} \cos(k_z^{P3} h) & i\mu_3 \Gamma_3 \sin(k_z^{S3} h) & \mu_3 \Gamma_3 \cos(k_z^{S3} h) \end{bmatrix}, \quad (24)$$

and where $\Omega_3 = \lambda_3 [(k_x)^2 + (k_z^{P3})^2] + 2\mu_3 (k_z^{P3})^2$, $\Gamma_3 = (k_z^{S3})^2 - (k_x)^2$, and λ_3 and μ_3 are Lamé constants of the layer 3.

We next propose x - and z -components of displacement (D_{x2} and D_{z2}) and stress (S_{x2} and S_{z2}) for the upper interface of the middle layer ($u_P = u_{P2}$ and $u_S = u_{S2}$)

$$\begin{bmatrix} D_{x2} \\ D_{z2} \\ S_{x2} \\ S_{z2} \end{bmatrix} = G_2 \begin{bmatrix} A_{rP2} + A_{tP2} \\ A_{rP2} - A_{tP2} \\ B_{rS2} - B_{tS2} \\ B_{rS2} + B_{tS2} \end{bmatrix} \exp [i (k_x x - \omega t)], \quad (25)$$

where

$$G_2 = \begin{bmatrix} ik_x \cos(k_z^{P2} z) & -k_x \sin(k_z^{P2} z) & -ik_z^{S2} \cos(k_z^{S2} z) & k_z^{S2} \sin(k_z^{S2} z) \\ -k_z^{P2} \sin(k_z^{P2} z) & ik_z^{P2} \cos(k_z^{P2} z) & -k_x \sin(k_z^{S2} z) & ik_x \cos(k_z^{S2} z) \\ -\Omega_2 \cos(k_z^{P2} z) & -i\Omega_2 \sin(k_z^{P2} z) & -2\mu_2 k_x k_z^{S2} \cos(k_z^{S2} z) & -2i\mu_2 k_x k_z^{S2} \sin(k_z^{S2} z) \\ -2i\mu_2 k_x k_z^{P2} \sin(k_z^{P2} z) & -2\mu_2 k_z^{P2} k_x \cos(k_z^{P2} z) & i\mu_2 \Gamma_2 \sin(k_z^{S2} z) & \mu_2 \Gamma_2 \cos(k_z^{S2} z) \end{bmatrix}, \quad (26)$$

and where $\Omega_2 = \lambda_2 [(k_x)^2 + (k_z^{P2})^2] + 2\mu_2 (k_z^{P2})^2$, $\Gamma_2 = (k_z^{S2})^2 - (k_x)^2$, and λ_2 and μ_2 are Lamé constants of the layer 2.

We finally derive x - and z -components of displacement (D_{x1} and D_{z1}) and stress (S_{x1} and S_{z1}) for the upper interface of the layer 1 ($u_P = u_{P1}$ and $u_S = u_S$)

$$\begin{bmatrix} D_{x1} \\ D_{z1} \\ S_{x1} \\ S_{z1} \end{bmatrix} = G_1^{z=0} \begin{bmatrix} A_{tP1} \\ -A_{tP1} \\ -B_{tS1} \\ B_{tS1} \end{bmatrix} \exp [i (k_x x - \omega t)], \quad (27)$$

where

$$G_1^{z=0} = \begin{bmatrix} ik_x & 0 & -ik_z^{S_1} & 0 \\ 0 & ik_z^{P_1} & 0 & ik_x \\ -\Omega_1 & 0 & -2\mu_1 k_x k_z^{S_1} & 0 \\ 0 & -2\mu_1 k_x k_z^{P_1} & 0 & \mu_1 \Gamma_1 \end{bmatrix}, \quad (28)$$

and where $\Omega_1 = \lambda_1 [(k_x)^2 + (k_z^{P_1})^2] + 2\mu_1 (k_z^{P_1})^2$, $\Gamma_1 = (k_z^{S_1})^2 - (k_x)^2$, and λ_1 and μ_1 are Lamé constants of the layer 1.

The displacement and stress are continuous at the interface, hence, we combine equations 23 - 27 to obtain

$$G_3^{z=h} \begin{bmatrix} A_{rP_3} + A_{iP} \\ A_{rP_3} - A_{iP} \\ B_{rS_3} \\ B_{tS_3} \end{bmatrix} = (G_2^{z=h}) (G_2^{z=0})^{-1} (G_1^{z=0}) \begin{bmatrix} A_{tP_1} \\ -A_{tP_1} \\ -B_{tS_1} \\ B_{tS_1} \end{bmatrix}. \quad (29)$$

Definitions of reflection and transmission coefficients in terms of wave amplitude, we rewrite equation 29 as

$$\begin{bmatrix} F_{11} + F_{12} & F_{13} + F_{14} & E_{12} - E_{11} & E_{13} - E_{14} \\ F_{21} + F_{22} & F_{23} + F_{24} & E_{22} - E_{21} & E_{23} - E_{24} \\ F_{31} + F_{32} & F_{33} + F_{34} & E_{32} - E_{31} & E_{33} - E_{34} \\ F_{41} + F_{42} & F_{43} + F_{44} & E_{42} - E_{41} & E_{43} - E_{44} \end{bmatrix} \begin{bmatrix} R_{PP} \\ R_{PS} \\ T_{PP} \\ T_{PS} \end{bmatrix} = \begin{bmatrix} F_{12} - F_{11} \\ F_{22} - F_{21} \\ F_{32} - F_{31} \\ F_{42} - F_{41} \end{bmatrix}, \quad (30)$$

where $E = (G_2^{z=h}) (G_2^{z=0})^{-1} (G_1^{z=0})$, $F = (G_3^{z=h})$, $R_{PP} = A_{rP_3}/A_{iP}$ is the P-wave reflection coefficient, $R_{PS} = B_{rS_3}/A_{iP}$ is the S-wave reflection coefficient, $T_{PP} = A_{tP_1}/A_{iP}$ is the P-wave transmission coefficient, and $T_{PS} = B_{tS_1}/A_{iP}$ is the S-wave transmission coefficient.

In order to calculate the quantities k_x , $k_z^{P_2}$ and $k_z^{S_2}$, P- and S-wave velocities \widetilde{V}_P and \widetilde{V}_S in the fractured and attenuative layer are needed. Schoenberg and Douma (1988) presented the P- and S-wave velocities in terms of two dimensionless compliances that are approximately equal to the normal and tangential fracture weaknesses in the case that the dimensionless compliances are small. Following Chichinina et al. (2006), we present the complex P- and S-wave velocities in terms of the attenuation factor and the normal fracture weakness

$$\begin{aligned} (\widetilde{V}_P)^2 &\approx \frac{M}{\rho} \left[1 - (1 - 2g \sin^2 \vartheta)^2 \widetilde{\Delta}_N - g (\sin 2\vartheta)^2 \widetilde{\Delta}_T \right] \\ &= \frac{M}{\rho} \left[1 - (1 - 2g \sin^2 \vartheta)^2 \Delta_N - g (\sin 2\vartheta)^2 \Delta_T \right] \\ &\quad + i \frac{M}{\rho} \left[(1 - 2g \sin^2 \vartheta)^2 \frac{1 - \Delta_N}{Q_N} \right], \end{aligned}$$

$$\begin{aligned}
 \left(\widetilde{V}_S\right)^2 &\approx \frac{\mu}{\rho} \left[1 - g (\sin 2\vartheta)^2 \widetilde{\Delta}_N - (\cos 2\vartheta)^2 \widetilde{\Delta}_T\right] \\
 &= \frac{\mu}{\rho} \left[1 - g (\sin 2\vartheta)^2 \Delta_N - (\cos 2\vartheta)^2 \Delta_T\right] \\
 &\quad + i \frac{\mu}{\rho} \left[g (\sin 2\vartheta)^2 \frac{1 - \Delta_N}{Q_N} \right],
 \end{aligned} \tag{31}$$

where ϑ is the angle between the wavenumber vector and the x_3 -axis (Schoenberg and Douma, 1988). The relationship among the angle ϑ , the incidence angle θ and the azimuthal angle φ is

$$\cos \vartheta = \sin \theta \cos \varphi. \tag{32}$$

Combining equations 9-12, we may estimate the attenuation factor and fracture weaknesses given fracture properties and fluid parameters. Using the estimated results, we calculate the complex P- and S-wave velocities using equations 31 and 32, and then we may compute the frequency-dependent reflection coefficient using the extended reflectivity modeling method.

NUMERICAL RESULTS

Variations of fracture weaknesses and attenuation factors with fracture properties and fluid parameters

We next analyze how fracture properties and fluid parameters affect the normal fracture weakness and the attenuation factor for the case of fractured and oil-bearing carbonate rocks. We assume minerals making up the rock to be calcite and clay (Clay content is 0.1), and fluid to be a homogeneous mixture of oil and water. We use the Voigt-Ruess-Hill average model (Mavko et al., 2009) to calculate the bulk and shear moduli of minerals, and we employ Krief et al. (1990) model to compute the effective moduli of the dry host rock. Table 1 shows mineral bulk and shear moduli, fluid moduli and viscosity.

Table 1. Bulk and shear moduli of minerals and fluids (Rops, 2017).

	K (GPa)	μ (GPa)	η_f (cp)
Calcite	76.8	32	-
Clay	25	9	-
Water	2.34	0	1
Oil	1.8	0	8

The tangential fracture weakness Δ_T is not influenced by fluid type (Bakulin et al., 2000; Chen et al., 2017c). In the present study, we show variations of the normal fracture weakness Δ_N and the attenuation factor $1/Q_N$ with frequency given different values of fracture density and water saturation, as shown in Figure 2.

From the variation of Δ_N , we observe that the normal fracture weakness increases with fracture density. The normal fracture weakness for a oil saturated rock is lower than that for a water saturated rock, and from the change of $1/Q_N$, we find that a larger fracture density

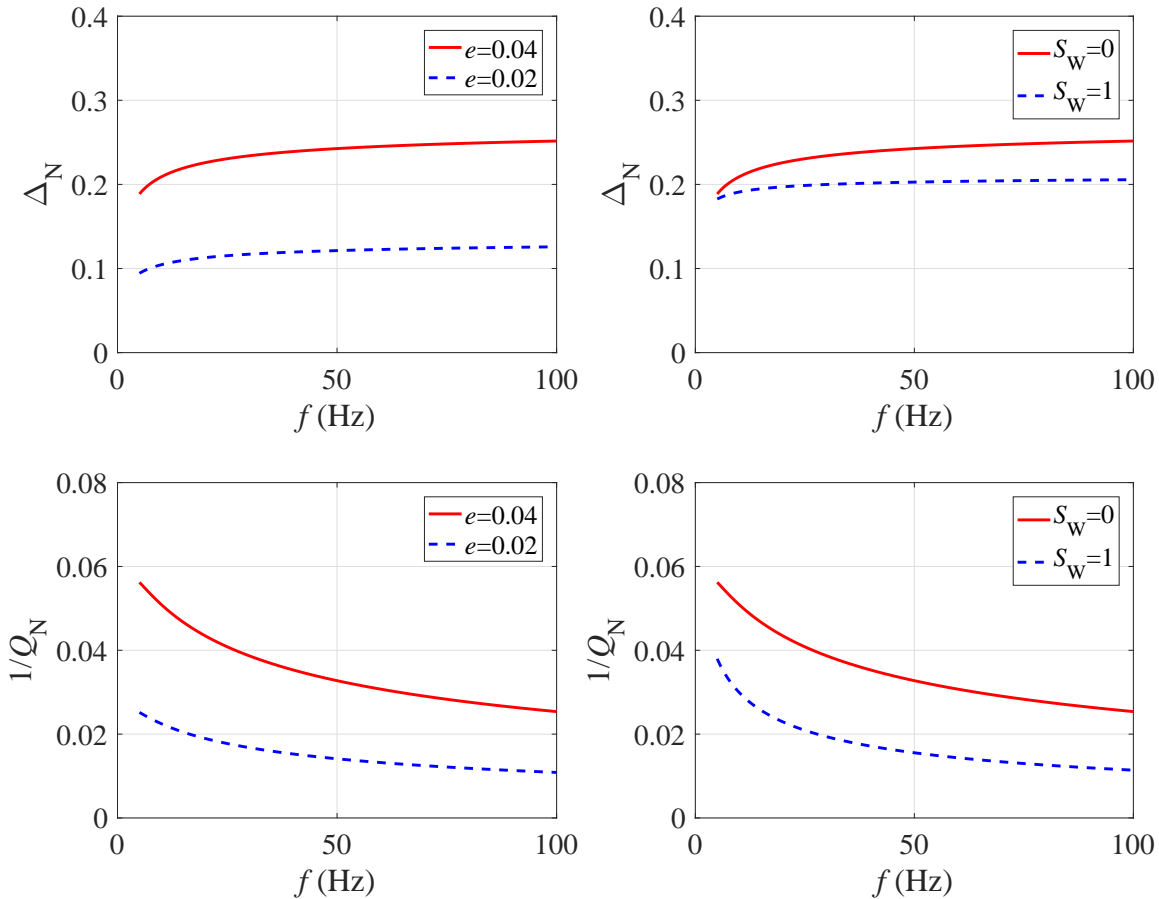


FIG. 2. Variation of the normal fracture weakness and the attenuation factor with frequency given different values of fracture density and water saturation. The fracture aspect ratio $c/a = 0.005$, the host rock permeability $P_m = 0.01\text{md}$, and the host rock porosity $\phi_h = 0.02$.

induces a stronger attenuation, and the fracture induced attenuation for a oil saturated rock is higher than that for a water saturated rock. We next plot the absolute value of relative difference between the water and oil saturated fractured rocks for Δ_N and $1/Q_N$, respectively (See Figure 3). We observe that the relative change in the attenuation factor is relatively larger than that in the normal fracture weakness, which indicates that the attenuation factor can be used as an indicator to discriminate oil-bearing fractured reservoirs.

Verification of the accuracy of linearized reflection coefficient

We use equation 17 and the extended reflectivity modeling method to calculate PP-wave reflection coefficient respectively to verify the accuracy of the derived linearized reflection coefficient. Figure 4 shows a two-layer model, and the lower layer is fractured carbonate rock in which mineral volumes, density, fracture properties and fluid parameters are displayed. Combining equations 9-12, we first compute the normal fracture weakness and the attenuation quality factor, and then calculate the frequency-dependent PP-wave reflection coefficient, after which we utilize the inverse Fourier transform to obtain the reflection coefficient in time domain. Figure 5 plots PP-wave reflection coefficient calculated using the linearized reflection coefficient and the extended reflectivity modeling method. In

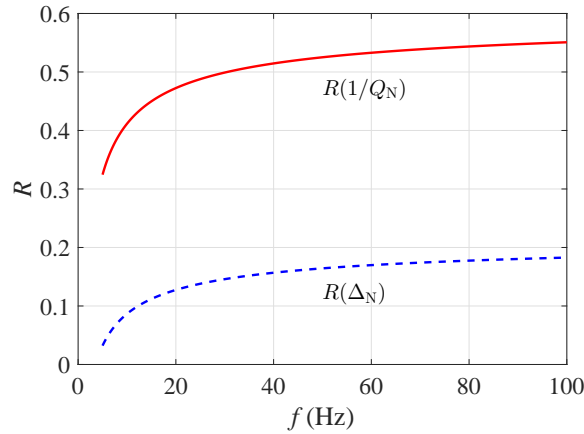


FIG. 3. Absolute value of relative difference between water and oil saturated rocks for the normal fracture weakness and the attenuation factor. The absolute value of relative difference is calculated using $R(x) = |(x_{oil} - x_{water})/x_{oil}|$, and x denotes Δ_N and $1/Q_N$, respectively.

this study, we assume types of the isotropic and elastic upper layer to be sand rock and carbonate rock, respectively. Table 2 shows parameters for the upper and lower layers.

Table 2. Parameters for the upper and lower layers.

	Upper (sand)	Upper (carbonate)	Lower (fractured carbonate)
M (GPa)	76	120	-
μ (GPa)	19	30	-
ρ (g/cm ³)	2.7	2.9	-
P_m (md)	-	-	0.001
ϕ_h	-	-	0.02

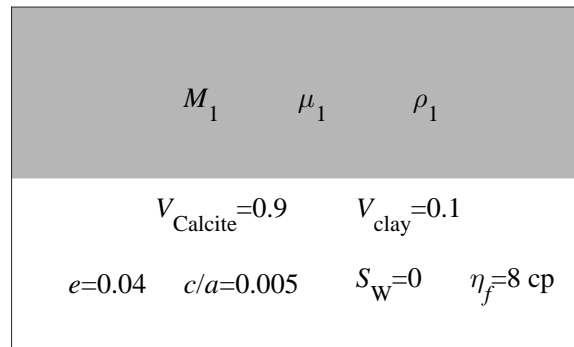


FIG. 4. Two-layer model for reflection coefficient calculation. For the second layer, the host rock permeability $P_m = 0.001md$, and the host rock porosity $\phi_h = 0.02$.

From Figure 5, we observe that the difference between the reflection coefficient calculated using the linearized equation and that computed using the extended reflectivity modeling method is relatively small in the case of the incidence angle θ being not much larger than 30° , which indicates that the derived linearized reflection coefficient is applicable to reflection response modeling in fractured and attenuative reservoirs. Hence, we may use the linearized reflection coefficient with a acceptable accuracy to obtain P-wave reflection response given different fracture properties and fluid parameters.

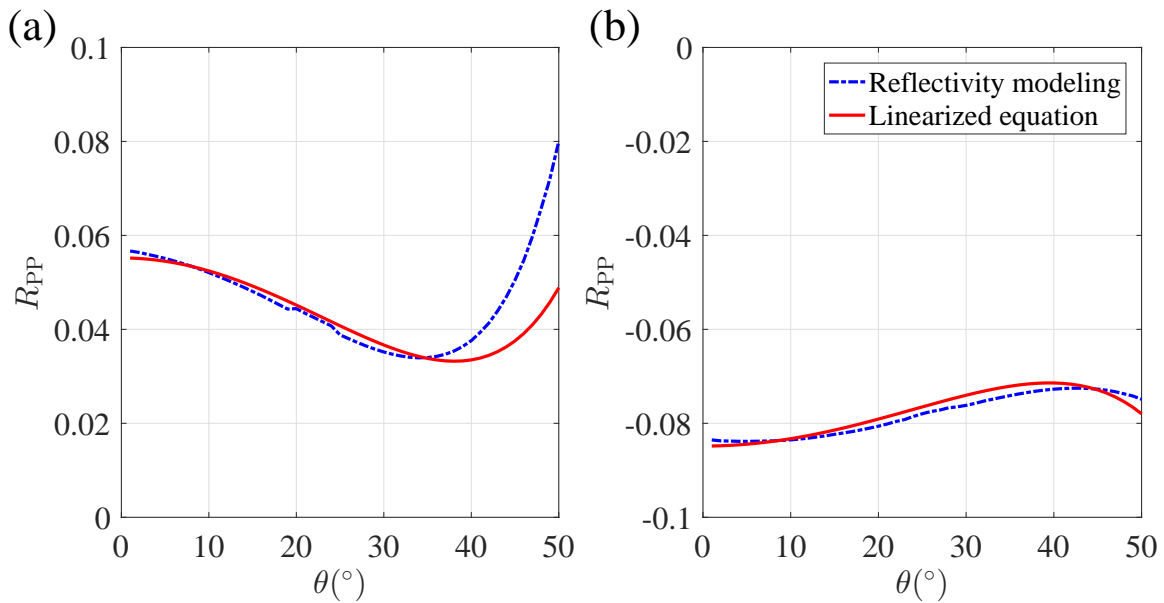


FIG. 5. Comparison between PP-wave reflection coefficient calculated using the linearized reflection coefficient and the extended reflectivity modeling method. (a) The upper layer is sand rock, and (b) The upper layer is carbonate rock.

Reflection response for oil-bearing carbonate rock

We proceed to forward modeling for PP-wave reflection coefficient using the derived linearized reflection coefficient in the case of different values of fracture density, water saturation and fluid viscosity. P- and S-wave moduli and density of the upper layer are $M = 60\text{GPa}$, $\mu = 15\text{GPa}$ and $\rho = 2.2\text{g/cm}^3$, and permeability and porosity of the host rock are $P_m = 0.001\text{md}$ and $\phi_h = 0.02$. We use a 35 Hz Ricker wavelet to generate seismic profiles for oil-bearing fractured and attenuative carbonate rocks with different values of fracture density, as shown in Figure 6.

We observe that the reflection amplitude difference between oil and water saturated fractured rocks increases with the incidence angle, and the reflection amplitude of oil saturated fractured rocks with different values of fracture density also increases with the incidence angle.

CONCLUSIONS

Based on the complex linear slip theory, we express the complex stiffness matrix in terms of fracture weaknesses and induced attenuation factor under the assumption of the host rock being elastic and isotropic. Incorporating with the attenuative crack model, we relate the induced attenuation factor to fracture properties (fracture density and aspect ratio) and fluid parameters (fluid bulk modulus and viscosity), and we also analyze the variation of the attenuation factor with fracture density and water saturation to verify the capability for distinguishing oil-bearing and water-bearing rocks. Using perturbations in the complex stiffness parameters, we derive a complex linearized reflection coefficient involving the induced attenuation factor and fracture weaknesses. We confirm that the derived reflection coefficient is applicable to the calculation of PP-wave reflection coefficient in the case of the

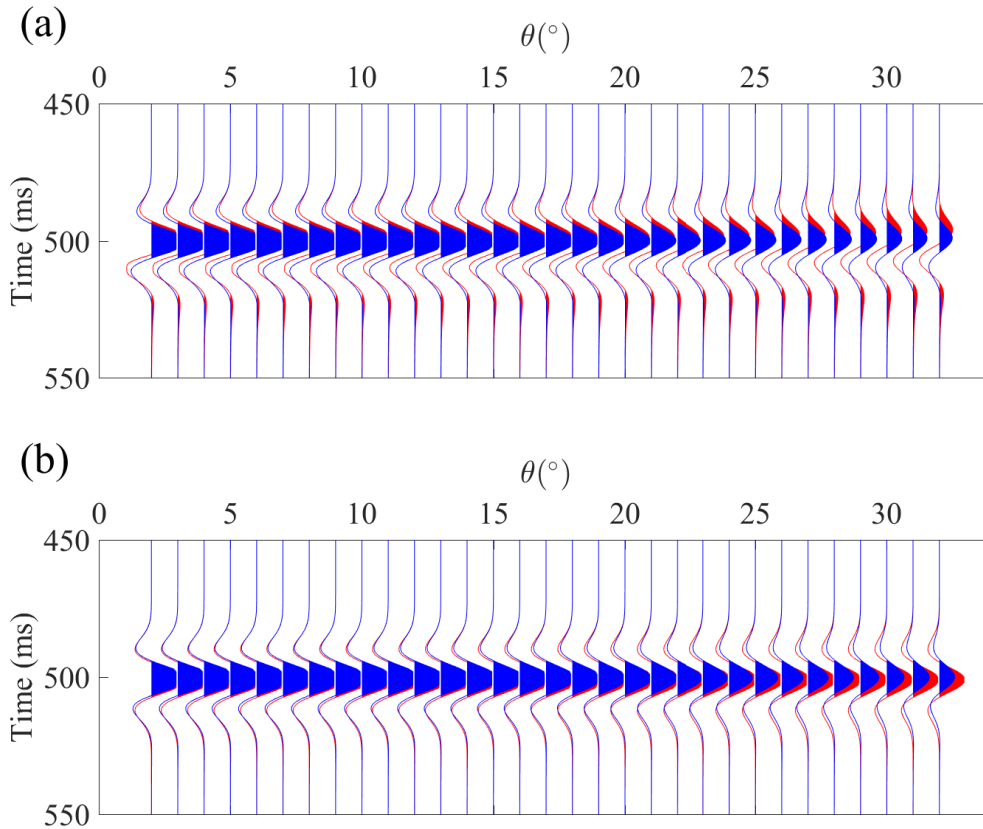


FIG. 6. Seismic profiles generated for oil-bearing fractured and attenuative rocks. (a) The blue color represents the case of oil saturated rock (i.e. $S_W = 0$), and red color represents the case of water saturated rock (i.e. $S_W = 1$); (b) The blue color represents the case of $e = 0.06$, and the red color represents the case of $e = 0.01$ for oil saturated fractured rock.

incidence angle being less than 30° . From the seismic response modeled using the derived reflection coefficient for fractured reservoirs with different values of fracture density and water saturation, we conclude that seismic response difference induced by fracture density and water saturation increases with the incidence angle.

ACKNOWLEDGEMENTS

The industrial sponsors of CREWES are thanked for their support. We gratefully acknowledge support from NSERC (Natural Science and Engineering Research Council of Canada) through the grant CRDPJ 461179-13. This research was undertaken thanks in part to funding from the Canada First Research Excellence Fund and Mitacs Project.

REFERENCES

- Bakulin, A., Grechka, V., and Tsvankin, I., 2000, Estimation of fracture parameters from reflection seismic data—part i: Hti model due to a single fracture set: *Geophysics*, **65**, No. 6, 1788–1802.
- Brajanovski, M., Müller, T. M., and Gurevich, B., 2006, Characteristic frequencies of seismic attenuation

- due to wave-induced fluid flow in fractured porous media: *Geophysical Journal International*, **166**, No. 2, 574–578.
- Carcione, J. M., 1992, Anisotropic q and velocity dispersion of finely layered media: *Geophysical Prospecting*, **40**, No. 7, 761–783.
- Carcione, J. M., 2000, A model for seismic velocity and attenuation in petroleum source rocks: *Geophysics*, **65**, No. 4, 1080–1092.
- Carcione, J. M., Gurevich, B., Santos, J. E., and Picotti, S., 2013, Angular and frequency-dependent wave velocity and attenuation in fractured porous media: *Pure and Applied Geophysics*, **170**, No. 11, 1673–1683.
- Carcione, J. M., Santos, J. E., and Picotti, S., 2012, Fracture-induced anisotropic attenuation: *Rock mechanics and rock engineering*, **45**, No. 5, 929–942.
- Chapman, M., 2003, Frequency-dependent anisotropy due to meso-scale fractures in the presence of equant porosity: *Geophysical Prospecting*, **51**, No. 5, 369–379.
- Chen, H., Ji, Y., and Innanen, K. A., 2017a, Estimation of modified fluid factor and dry fracture weaknesses using azimuthal elastic impedance: *Geophysics*, **83**, No. 1, 1–74.
- Chen, H., Pan, X., Ji, Y., and Zhang, G., 2017b, Bayesian markov chain monte carlo inversion for weak anisotropy parameters and fracture weaknesses using azimuthal elastic impedance: *Geophysical Journal International*, **210**, No. 2, 801–818.
- Chen, H., Zhang, G., Ji, Y., and Yin, X., 2017c, Azimuthal seismic amplitude difference inversion for fracture weakness: *Pure and Applied Geophysics*, **174**, No. 1, 279–291.
- Chichinina, T., Obolentseva, I., Gik, L., Bobrov, B., and Ronquillo-Jarillo, G., 2009, Attenuation anisotropy in the linear-slip model: Interpretation of physical modeling data: *Geophysics*, **74**, No. 5, WB165–WB176.
- Chichinina, T., Sabinin, V., and Ronquillo-Jarillo, G., 2006, Qvoa analysis: P-wave attenuation anisotropy for fracture characterization: *Geophysics*, **71**, No. 3, C37–C48.
- Galvin, R., and Gurevich, B., 2009, Effective properties of a poroelastic medium containing a distribution of aligned cracks: *Journal of Geophysical Research: Solid Earth*, **114**, No. B7.
- Gurevich, B., 2003, Elastic properties of saturated porous rocks with aligned fractures: *Journal of Applied Geophysics*, **54**, No. 3, 203–218.
- Hudson, J., 1980, Overall properties of a cracked solid, *in* *Mathematical Proceedings of the Cambridge Philosophical Society*, vol. 88, Cambridge University Press, 371–384.
- Hudson, J., Liu, E., and Crampin, S., 1996, The mechanical properties of materials with interconnected cracks and pores: *Geophysical Journal International*, **124**, No. 1, 105–112.
- Kong, L., Gurevich, B., Müller, T. M., Wang, Y., and Yang, H., 2013, Effect of fracture fill on seismic attenuation and dispersion in fractured porous rocks: *Geophysical Journal International*, **195**, No. 3, 1679–1688.
- Krief, M., Garat, J., Stellingwerf, J., and Ventre, J., 1990, A petrophysical interpretation using the velocities of p and s waves (full-waveform sonic): *The Log Analyst*, **31**, No. 06.
- Mavko, G., Mukerji, T., and Dvorkin, J., 2009, *The rock physics handbook: Tools for seismic analysis of porous media*: Cambridge university press.
- Pointer, T., Liu, E., and Hudson, J. A., 2000, Seismic wave propagation in cracked porous media: *Geophysical Journal International*, **142**, No. 1, 199–231.
- Rops, E., 2017, Predicting heavy oil and bitumen viscosity from well logs and calculated seismic properties: M.Sc. thesis, University of Calgary.

- Schoenberg, M., and Douma, J., 1988, Elastic wave propagation in media with parallel fractures and aligned cracks: *Geophysical Prospecting*, **36**, No. 6, 571–590.
- Schoenberg, M., and Sayers, C. M., 1995, Seismic anisotropy of fractured rock: *Geophysics*, **60**, No. 1, 204–211.
- Shaw, R. K., and Sen, M. K., 2004, Born integral, stationary phase and linearized reflection coefficients in weak anisotropic media: *Geophysical Journal International*, **158**, No. 1, 225–238.
- Shaw, R. K., and Sen, M. K., 2006, Use of avoa data to estimate fluid indicator in a vertically fractured medium: *Geophysics*, **71**, No. 3, C15–C24.
- Tang, X.-M., Chen, X.-l., and Xu, X.-k., 2012, A cracked porous medium elastic wave theory and its application to interpreting acoustic data from tight formations: *Geophysics*.
- Zhu, T., 2017, Numerical simulation of seismic wave propagation in viscoelastic-anisotropic media using frequency-independent q wave equation: *Geophysics*, **82**, No. 4, WA1–WA10.